



ANRCP-1999-5
February 1999

Amarillo National Resource Center for Plutonium

A Higher Education Consortium of The Texas A&M University System,
Texas Tech University, and The University of Texas System

Design, Construction, Establishment of Proof of Principle, and Testing of a Spectrometer to Permit Spectroelectrochemical Investigations of Actinides in a Confined System

Purnendu K. Dasgupta and Jianzhong Li
Department of Chemistry and Biochemistry
Texas Tech University

This report was prepared with the support of the U.S. Department of Energy (DOE) Cooperative Agreement No. DE-FC04-95AL85832.

However, any opinions, findings, conclusions, or recommendations expressed herein are those of the author(s) and do not necessarily reflect the views of DOE. This work was conducted through the Amarillo National Resource Center for Plutonium.

Edited by

Angela L. Woods
Technical Editor

600 South Tyler • Suite 800 • Amarillo, TX 79101
(806) 376-5533 • Fax: (806) 376-5561
<http://www.pu.org>

AMARILLO NATIONAL RESOURCE CENTER FOR PLUTONIUM/
A HIGHER EDUCATION CONSORTIUM

A Report on

**Design, Construction, Establishment of Proof of Principle, and Testing of a Spectrometer to
Permit Spectroelectrochemical Investigations of Actinides in a Confined System**

Purnendu K. Dasgupta and Jianzhong Li
Department of Chemistry and Biochemistry
Texas Tech University
Lubbock, Texas 79409

Submitted for publication to

ANRC Nuclear Program

February 1999

Design, Construction, Establishment of Proof of Principle, and Testing of a Spectrometer To Permit Spectroelectrochemical Investigations of Actinides in a Confined System

Purnendu K. Dasgupta and Jianzhong Li
Department of Chemistry and Biochemistry

Abstract

This study examines the design, construction, and performance of a spectrometer that was designed and built for UV-visible absorption spectroscopic studies in molten salt media.

Contrary to previous designs in the literature, we found that furnace and chemical components can be located away from the instrument and electronics. In studying the performance of the spectrometer, we used a

potassium chloride eutectic mixture as the molten salt medium. We found that UV-visible absorption spectroscopic studies can be conveniently created in a molten alkali halide media with inexpensive equipment coupled with good sensitivity and precision. Further research will focus on designing a suitable fiber optic probe that will allow us to monitor the molten salt process on-line.

TABLE OF CONTENTS

1. CONSTRUCTION OF THE SPECTROMETER	1
1.1 Furnace Designs	1
1.2. Optical Cell	1
1.3 Monochromator and Detector	1
2. PERFORMANCE OF THE SPECTROMETER	3
2.1 Heater Characteristics	3
2.2 Noise Level	3
2.3 Wavelength Range	3
2.4 Optical Cell Uniformity and Corrosion Problems	3
2.5 Absorbance Linearity	4
3. SPECTROPHOTOMETRIC STUDIES OF SOME METAL CHLORIDES IN MOLTEN SALT MEDIA	5
3.1 CoCl ₂ in Concentrated Aqueous Chloride Solutions vs. Molten Salt Media	5
3.2 CuCl ₂ and CuCl in Molten NaCl and KCl Media	6
3.3 NiCl ₂ in Concentrated Aqueous Chloride Solutions vs. Molten Salt Media	6
4. CONCLUSIONS	9

LIST OF FIGURES

Figure 1a: Furnace Design Shown with a Circular Tube.....	13
Figure 1b: Spectrometer Design	14
Figure 2: Observed Background “Blackbody” Radiation vs. Source Light Intensity.....	15
Figure 3a: Time-Temperature Profile in Furnace Turn-On	16
Figure 3b: Time Required to Melt and Remelt Salt Mixtures	17
Figure 4a: Spectra of CoCl_2 in Molten NaCl-KCl Eutectic at Various Concentrations	18
Figure 4b: Beer’s Law Plot for 608 nm for Data in Figure 4a.....	19
Figure 5a: Spectra of CoCl_2 in Various Concentrations of LiCl	20
Figure 5b: Cobalt(II)-Chloride Complexation Model	21
Figure 6a: Spectra of CuCl_2 in NaCl-KCl Melt Immediately after Melting at Various Concentrations of Cu(II)	22
Figure 6b: Spectra of CuCl in Molten NaCl-KCl	23
Figure 6c: Change in Spectral Characteristics of CuCl_2 after Holding for Various Periods at 800°C	24
Figure 6d: First Order Decomposition Data for CuCl_2	25
Figure 7: Spectra of NiCl_2 in NaCl Melt and 2 M NaCl Solution	26

1. CONSTRUCTION OF THE SPECTROMETER

The design of the spectrometer for molten salt study is shown as Figure 1 (a and b). A Xenon flash lamp (EG&G, LS 1130 Flashpac, using a high power, UV window flashlamp, FX 1151, EG&G Electro-Optics Division, Salem, MA) is used as light source. An external TTL output trigger source is used to fire the lamp at any desired frequency. The light is coupled to an extended UV transmission optical fiber (silica core, 1mm in ID), the furnace end of which is encased in ceramic tubing. A similar arrangement is used for conducting the light transmitted through the molten salt sample.

1.1 Furnace Designs

The high-temperature furnace design is based on a commercial available small furnace heater that is 6 inches long, contains a ½ inch central cavity and is 2 inches in outside diameter (see Figure 1, Furnace: Ceramic Fiber Heater, Model # UC400J06A-A007R, Watlow Electric, St. Louis, MO). Rated at only 175W, the cavity of this heater can be heated to 1200°C. With two to three inches of additional ceramic fiber insulation on the exterior, the outer container wall can be kept at ~100°C or less. The furnace is modified slightly to meet the need of the optical furnace. One hole was drilled diametrically, and then two pieces of the ceramic tube which were used to hold the optical fibers were cemented in place using high temperature cement (Omega Engineering, Stamford, CT). Another hole was drilled to accommodate the thermocouple (Part No. AFEA0TQ010GK06H (Watlow-Gordon). The thermocouple output is read and displayed by a temperature controller (Auto-tuning control 965A-3FA0-00RG (Watlow Controls) with an attendant solid state power controller (DIN-a-mite, Style A, Watlow Controls) applied to the furnace.

The cladding from the first three inches of each of the optical fibers is removed because the cladding will not withstand the temperature. However, within this short transmission distance, major light loss is not expected.

1.2 Optical Cell

Fused silica tubes were used to prepare the optical cell. Each cell is about 6 inches long, and one end of the tube is sealed. A quartz rod is joined as a handle towards the top of each cell, so that they can be handled easily at high temperatures.

Cells were made from two type of tubes, circular and square. The square cross-section tubes exhibited much better run-to-run reproducibility and absorbance linearity than cells with a round cross-section. Cells with square cross section (5 mm and 7 mm inner dimension, 1.3 mm wall thickness each, QS 105 and QS 107, respectively, Vitrocom, Mountain Lakes, NJ) were henceforth used in the molten salt studies. Results reported are those obtained with the QS 107 tubes.

It should be noted that the optical clarity of fused vitreous silica is lost upon prolonged use with molten alkali halides, presumably due to diffusion of alkali metal ions into the silica matrix. However, this does not pose any problems in carrying out short-term experiments; continuously prolonged exposure on experiments also pose no problems because the opacity is only observed after a cooling cycle.

1.3 Monochromator and Detector

The monochromator and the photodiode array detector (Control Development Inc., South Bend, IN) is integrated into an ISA-bus card that plugs into a full size slot of a personal computer (Pentium II class, 233 MHz). The spectrometer (CDIPDA 200-800. 1.2 nm resolution per pixel) is a single beam device with a high degree of wavelength stability.

All parameters related to spectroscopic measurement, such as integration time, acquisition of reference or background spectra and automated/sequential data collection and display can be controlled and manipulated by vendor supplied software (or minor modification thereof). For some cases, more intensive data processing were carried out by exporting the data to a spreadsheet (MS Excel) and using its mathematical/statistical capabilities.

2. PERFORMANCE OF THE SPECTROMETER

2.1 Heater Characteristics

In absorption spectroscopy, we are interested in looking solely at the attenuation of source light. Contribution of light from other than the intended source can compromise photometric and spectral accuracy. One of the problems related to heater design is the incandescence of the heat element that is visible to the spectrometer. Presently we simply heat it past the intended temperature and then turn off the heater until it comes down to the intended temperature; a very short time is required to acquire a spectrum or multiple spectra. The background radiation problem is also solved by increasing the source intensity relative to the background. We selected a pulsed Xe flash lamp from EG&G that delivers 0.1 joules per pulse that is 0.5 microseconds wide. The pulse can be repeated at rates exceeding 100 Hz, resulting in an effective CW power of ~10 W.

However the peak power when the pulse occurs is 200 KW. If we narrow our temporal viewing window, we have a very large discrimination factor over the blackbody radiation. Presently we can easily acquire the spectrometric data in 1 ms, it could possibly be done in a much shorter period. Even with an 1 ms integration, the effective CW power is 100 W, much above the blackbody radiation background (see Figure 2).

The system can reach the required temperature quickly; for example, when the temperature is set to 800°C, it takes 90 seconds to reach that temperature from ambient conditions after turning on the furnace (Figure 3a). At this temperature, an equimolar mixture of NaCl and KCl, kept in the fused silica cell, melts completely. It is interesting to note that the salt mixture melts in ≤ 3 minutes the first time but remelting takes a significantly longer time, ~6 minutes

(Figure 3b); possibly this is caused by less efficient heat transport.

2.2 Noise Level

In order to test the intrinsic signal to noise level of the spectrometer, a stable light emitting diode (LED) source at room temperature was used to test the absolute photometric stability of the spectrophotometer system. Based on 8 repeated spectral acquisitions with one second integration, the standard deviation was computed to be 0.05789% in intensity which corresponds to an absorbance noise level of 0.00025 absorbance units (250 μ AU). If one source wavelength was referenced to another to compensate for source intensity fluctuations, the absorbance noise was found to be 180 μ AU. The corresponding noise level on the Xe flash lamp with the self-referencing procedure was found to be virtually the same as the stable LED source, 200 μ AU.

2.3 Wavelength Range

The wavelength range of the spectrometer depends on the monochromator, detector and the type of the optical fiber used. When silica optical fibers are used, the spectra in the range of 280nm to 1000nm can be obtained. However, because of interference from blackbody radiation, high sensitivity spectra (1 mAU resolution) can be acquired up to 600 nm and with substantially decreased sensitivity to 700 nm.

2.4 Optical Cell Uniformity and Corrosion Problems

The optical cell is made with fused quartz tubes; these are not of optical grade or flatness. The difference in surface flatness uniformity and other optical characteristics compromise the accuracy and reproducibility of absorbance measurements. The apparent optical difference among otherwise identically constructed cells was tested by measuring the absorbance of CoCl₂ solution

(10mg/mL) at 510nm. The maximum absorbance difference among 5 cells was 35 mAU in a mean absorbance level of 480 mAU. When using the same cell and the same solution as above, the maximum absorbance difference at 510 nm is 16 mAU during 6 repeated and repositioned measurements. This demonstrated that the main source of photometric error presently lies in the uniformity of the cells and the position of the cell in the furnace and not the S/N ratio of the spectrometer itself. Since the plans for 1999 call for the use of an immersible probe and the measurement through the cell walls are not involved, this factor will not be important, eventually.

It is interesting to note that the corrosive power of the vapor phase alkali halide is greater than that of the salt melt itself. It appears that the region immediately above the salt melt is more severely attacked than the area in actual contact with the molten salt. Even as the cell becomes optically opaque gradually with use, when salt is remelted in the cell, it becomes visibly transparent and

thus does not affect absorbance measurements. However, some metallic oxides, e.g., Fe_2O_3 and MnO_2 , etc., bind strongly to the quartz and penetrate significantly in to the wall at the high use temperatures. Such cells can neither be used further, nor is it possible to clean them for reuse.

2.5 Absorbance Linearity

Different amounts of CoCl_2 were incorporated in a molten NaCl and KCl eutectic salt mixture to obtain samples that contain 0.01% to 0.05% Co by weight in 0.01% increments. The mixtures are prepared by dropping in a solution and then drying the mixture in an oven. The absorption spectra were taken at 700°C (Figure 4a). The absorption at 608nm obeys Beer's law very well (Figure 4b). The regression equation is:

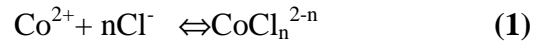
$$A=29.652C (\%Co) + 0.017, \text{ linear } r^2 = 0.9995).$$

3. SPECTROPHOTOMETRIC STUDIES OF SOME METAL CHLORIDES IN MOLTEN SALT MEDIA

In this study, a sodium chloride and potassium chloride eutectic mixture (mole ratio 1:1) was used as the molten salt medium. Various metal chlorides were added to the salt mixture with two different methods, and their spectra were studied. The first method involved the addition of a desired amount of the chloride salt of interest in solution to the NaCl-KCl salt mixture and dry in the oven after then. The second method was to weigh the metal chloride of interest directly and mix it with the salt mixture in the dry form. The first method was used for metal chlorides that are easily soluble in water or dilute HCl while the second method was used for metal chlorides that are insoluble under these conditions. CoCl₂, CuCl₂, CuCl, and NiCl₂ dissolve fully in molten NaCl-KCl medium. Addition of CrCl₃ and CeCl₃ to molten salt media cause brown and white precipitation, respectively. At the high temperatures of the medium and the convection currents introduced by the furnace, the solid material does not settle regardless of its density but is circulated around (the viscosity of molten salt at the operating temperature does not appear to be markedly different from that of water. As a result, while reproducible spectra can be obtained, it most likely represents a combination of the absorption spectra of the solution and the reflectance spectra of the floatsam. FeCl₃ decomposes in molten salt, forming a red sediment and leaving dense red and brown coloration in the cell walls that is very difficult to clean and reuse. SnCl₂ produce a yellow precipitate. Lanthanides such as EuCl₃, ErCl₃, SmCl₃, YCl₃ were studied. All produce white precipitates. Three detailed cases are described in the following sections.

3.1 CoCl₂ in Concentrated Aqueous Chloride solutions vs. Molten Salt Media

Figures 4a, b respectively shows the spectra of 0.01% to 0.05% by wt. Co in 0.01% increments in a molten NaCl-KCl medium and the beer's law plot for the same for the principal band at 608nm. It is of interest to look at the spectrum of CoCl₂ in aqueous chloride solutions (Figure 5a). LiCl, which has the highest solubility among alkali chlorides, was used in these experiments to attain as high a chloride concentration as possible. At low chloride concentration, the pink hexaaquo cobalt ion ($\lambda_{\max} \sim 500\text{nm}$) is the principal absorption band and as Cl⁻ concentration increase, the chlorocomplex ($(\lambda_{\max} \sim 600\text{nm})$ absorption band appears with increasing intensity. Modeling in terms of the absorbance at 600nm being solely due to the hexachlorocobalt(II) ion can be conducted as follows. The following is admittedly most simplistic, since computation of ionic activities in extremely concentrated salts or in salt melts still have no satisfactory *a priori* approaches. Here we have simply used concentrations, all concentrations (either in aqueous solution or in the salt melt being on the mole/kg basis). Let us further assume that in concentrated chloride media, it is sufficient to consider only the existence of the fully coordinated *n*-chlorocobalt(II) ion, i.e, the sole extant equilibrium being:



Where the cumulative stability constant β_n being:

$$\beta_n = [\text{CoCl}_n^{2-n}] / \{[\text{Co}^{2+}][\text{Cl}^{-}]^n\} \quad (2)$$

The total metal concentration M added to the system is present as either Co²⁺ or CoCl_n²⁻ⁿ whence:

$$M = [\text{Co}^{2+}] + [\text{CoCl}_n^{2-n}] \quad (3)$$

If the observed absorbance A in the 600 nm absorption band is ascribed solely to the CoCl_n^{2-n} species, the observed absorbance A would be given by:

$$A = \epsilon b[\text{CoCl}_n^{2-n}] \quad (4)$$

Where ϵ is the extinction coefficient in appropriate units and b is the optical pathlength in cm.

Using Equations (2) – (4) above, one obtains:

$$A = \beta_n M \epsilon b [\text{Cl}^-]^n / \{1 + \beta_n [\text{Cl}^-]^n\} \quad (5)$$

The available aqueous solution data that were obtained at chloride concentrations ranging from 0 to 9.2 mol/kg at an added cobalt concentration of 17.3-24.3 mmol/kg were fitted according to eqn 5 using the Solver function in MS Excel. A , M , b (0.7 cm for the cell used) and $[\text{Cl}^-]$ were input and the best fit values of n , β_n , and ϵ were ascertained. The value of n was constrained to be an integer and the best fit value was 6. The overall best fit ($\beta_6 = 2.9 \text{ E-}6$ and $\epsilon = 183 \text{ mol kg}^{-1} \text{ cm}^{-1}$) is shown in Figure 5b. Considering the extent of approximations made, the model fits the general observations well. Now if we take the absorbance at 608 nm for the 0.05% wt% CoCl_2 in the molten salt ($M = 8.5 \text{ mmol/kg}$), and put in the best fit values of n , β_n , and ϵ , one calculates $[\text{Cl}^-] = 7.6 \text{ mol/kg}$ whereas the actual concentration of chloride in a pure NaCl-KCl melt is 15 mol/kg. Alternatively, using the aqueous chloride data, one predicts an absorbance of 0.76 at 608 nm instead of the observed 0.386 for this cobalt concentration in the salt melt. All of the other absorbance data for different cobalt concentrations in the salt melt can be similarly predicted within a factor of two. Considering the great disparity in the actual temperature conditions of the two systems and the crudeness of the approximations

made, an agreement within a factor of two is remarkable.

3.2 CuCl_2 and CuCl in Molten NaCl and KCl Media.

CuCl_2 forms a visibly yellow solution in the molten NaCl-KCl eutectic, the maximum absorption appears to shift to longer wavelengths with increasing CuCl_2 concentration (Figure 6a). In contrast, CuCl shows a single, intense, well-defined absorption band centered at 320nm (Figure 6b). However, CuCl_2 in the molten salt medium appears to decompose over a period of time since the spectral characteristics change with time. It is known that if pure CuCl_2 is heated, it decomposes into CuCl and chlorine gas. The chloride complexation of Cu(I) is favored over that of Cu(II) ($\text{Cu(I)}: \log\beta_3=5.7$; $\text{Cu(II)}: \log\beta_3=0.79$). So from this perspective also, CuCl_2 should decompose to Cu(I) . The salt mixture containing 0.08% CuCl_2 was heated to the molten state and kept at 800 °C for different periods of time. Then the melt was allowed to cool and spectra were taken at a temperature of 600°C. The absorption band at 480 nm disappeared and the overall absorption shifted to shorter wavelengths as the time at 800°C was prolonged. Eventually, the original yellow color of the CuCl_2 disappeared completely and the absorption spectra became the same as CuCl (Figure 6c). During the study, the evolution of chlorine from the melt could be sensed from its distinct odor. The reaction appears to proceed at a first order rate, a plot of $\log(A_{500\text{nm}})$ with time at 800°C is linear with time (Figure 6d). At 800°C, the first order rate constant for the reaction is $9.3 \times 10^{-4} \text{ s}^{-1}$.

3.3 NiCl_2 in Concentrated Aqueous Chloride solutions vs. Molten Salt Media

NiCl_2 dissolves completely in the equimolar NaCl and KCl mixture. The

spectra of NiCl_2 in molten salt medium and 2M NaCl water solution are shown in Figure 7. It is interesting to note that many of the characteristic absorption bands in the molten salt media are same as those in aqueous chloride solutions.

4. CONCLUSIONS

We have demonstrated here that near UV-visible absorption spectroscopic studies can be made conveniently in molten alkali halide media with affordable inexpensive equipment but nevertheless with good sensitivity and precision. The spectrometer for molten salt studies developed in this work is compact, stable and simple. Because communication with the optical cell in the furnace is via optical fibers, the furnace and

the chemical components can be located away from the instrument and electronics, in contrast to extant designs in the literature. No additional thermal insulation on the commercial furnace is really necessary for routine operation. The whole system is flexible and easy to maintain. The next logical step will be to design a suitable fiber optic probe that will allow us to monitor the molten salt process on-line.

REFERENCES

There were no references cited for this report.

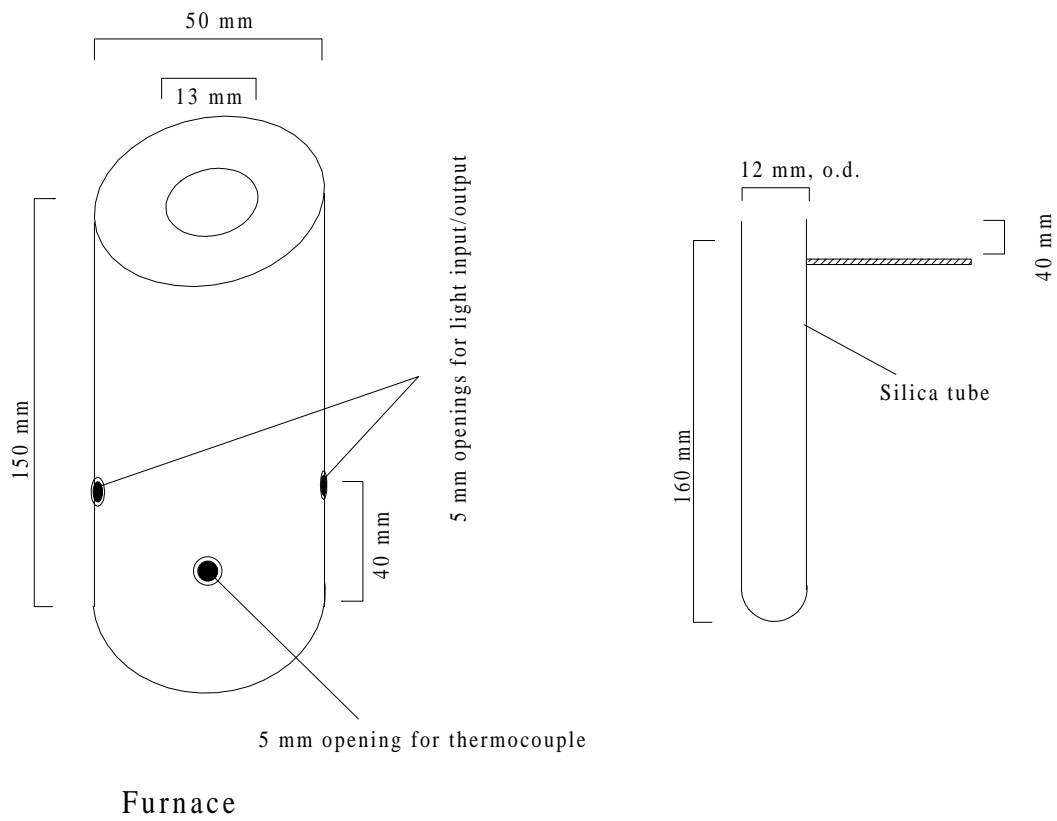
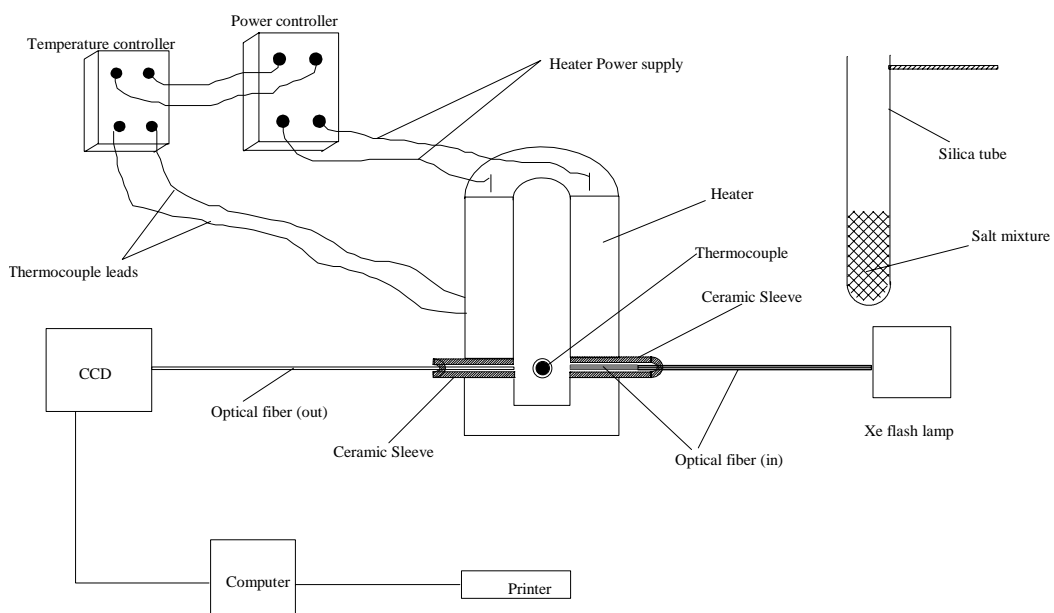


Figure 1a: Furnace Design Shown with a Circular Tube



Part Numbers:

- Furnace: Ceramic Fiber Heater, Model # UC400J06A-A007R (Watlow Electric)
- Power Controller: DIN-a-mite, Style A (Watlow Controls)
- Temperature Controller: Auto-tuning control 965A-3FA0-00RG (Watlow Controls)
- Thermocouple: AFEA0TQ010GK06H (Watlow-Gordon)
- Light Source: LS-1130 Flashpac (EG&G Electro-Optics)

Figure 1b: Spectrometer Design

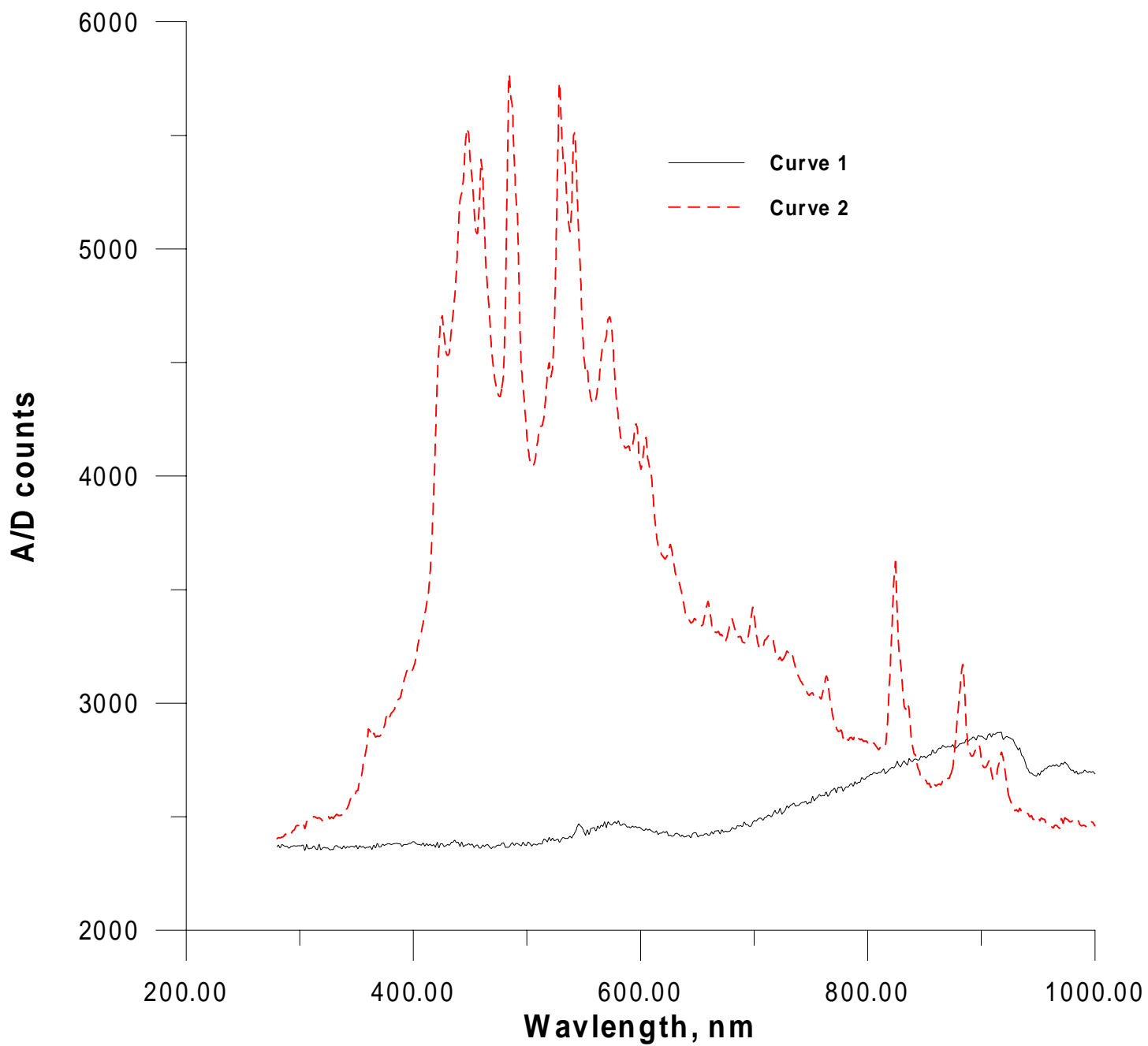


Figure 2: Observed Background “Blackbody” Radiation vs. Source Light Intensity

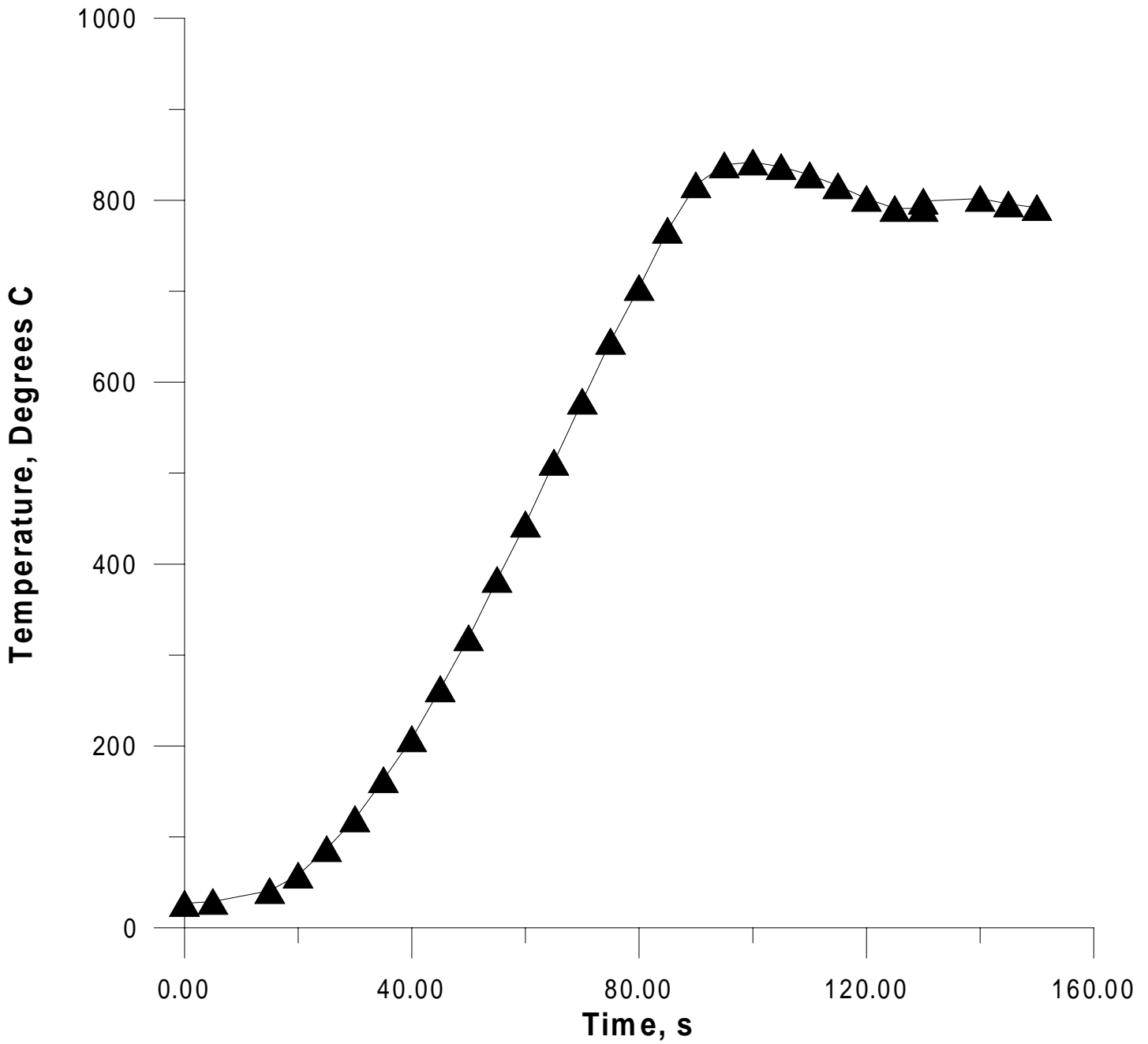


Figure 3a: Time-Temperature Profile in Furnace Turn-On

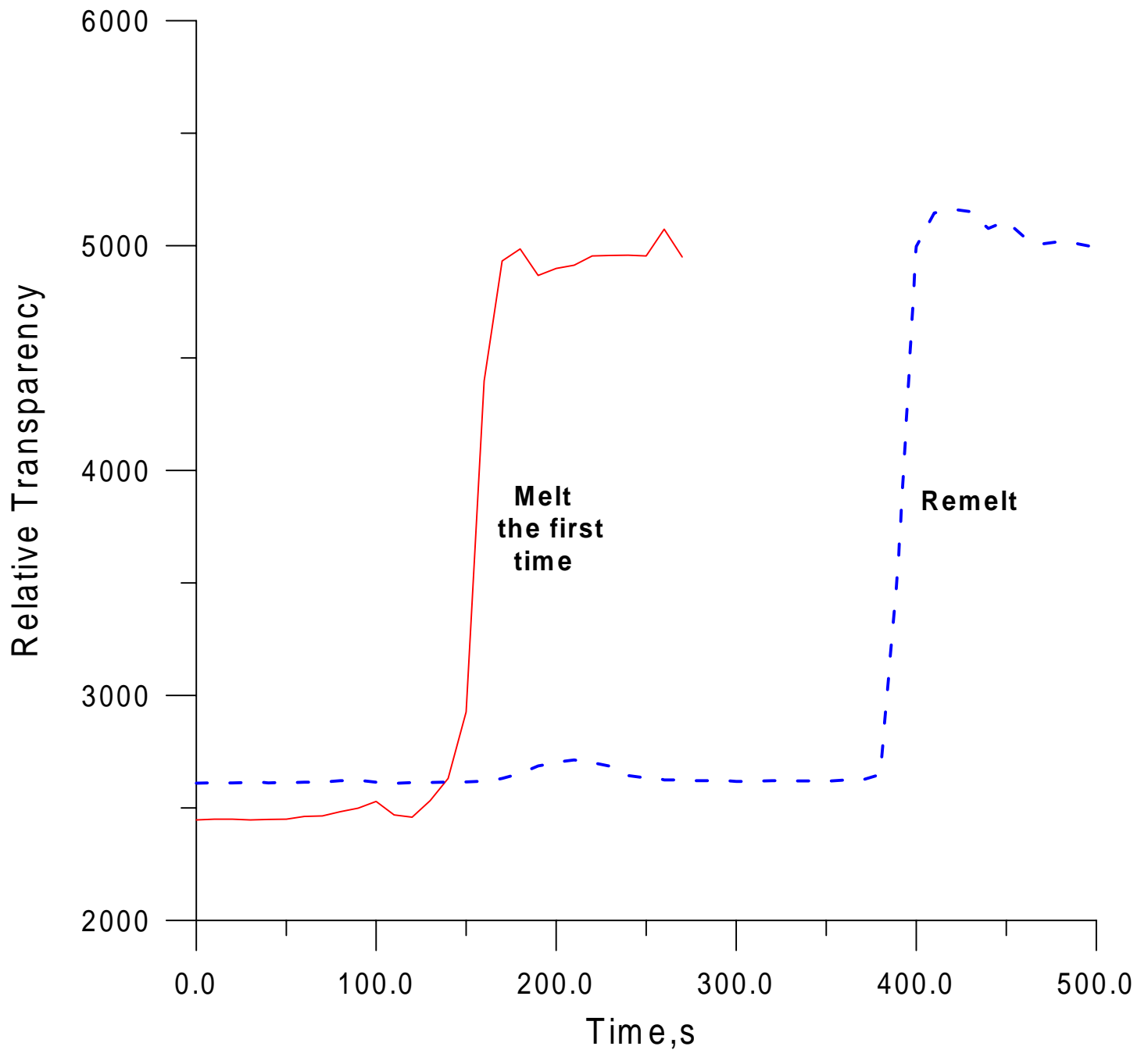


Figure 3b: Time Required to Melt and Remelt Salt Mixtures

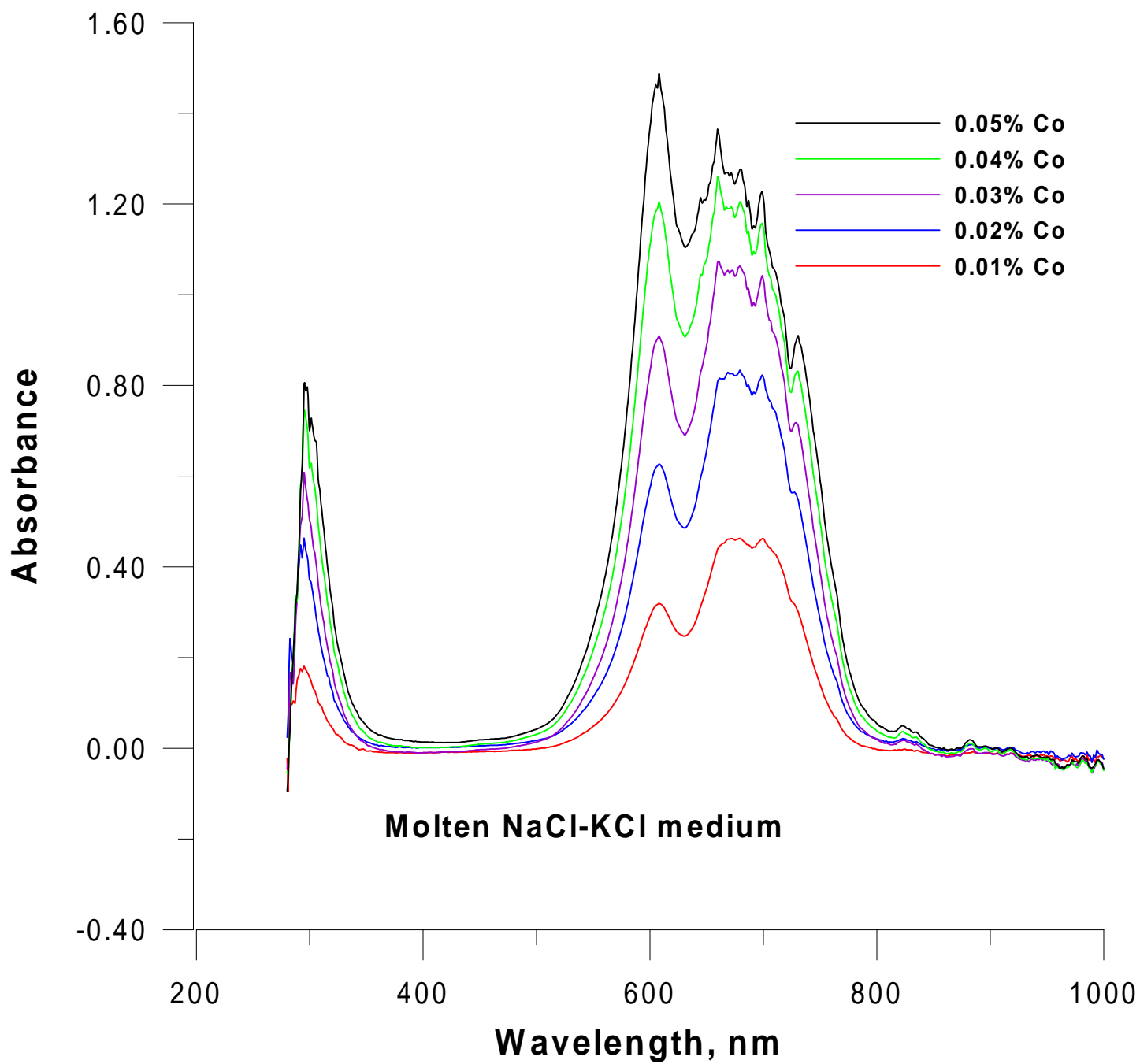


Figure 4a: Spectra of CoCl_2 in Molten NaCl-KCl Eutectic at Various Concentrations

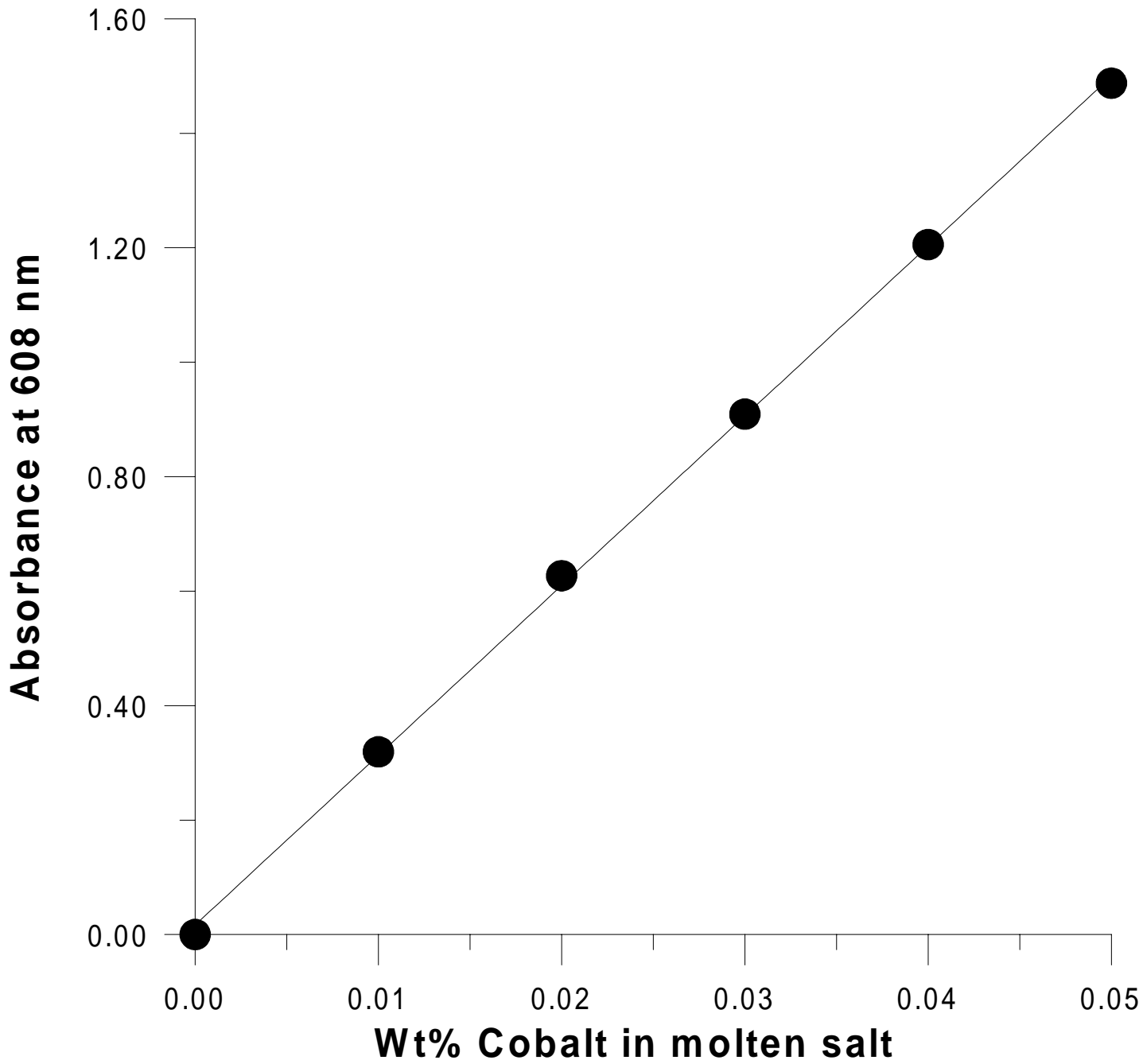


Figure 4b: Beer's Law Plot for 608 nm for the Data in Figure 4a

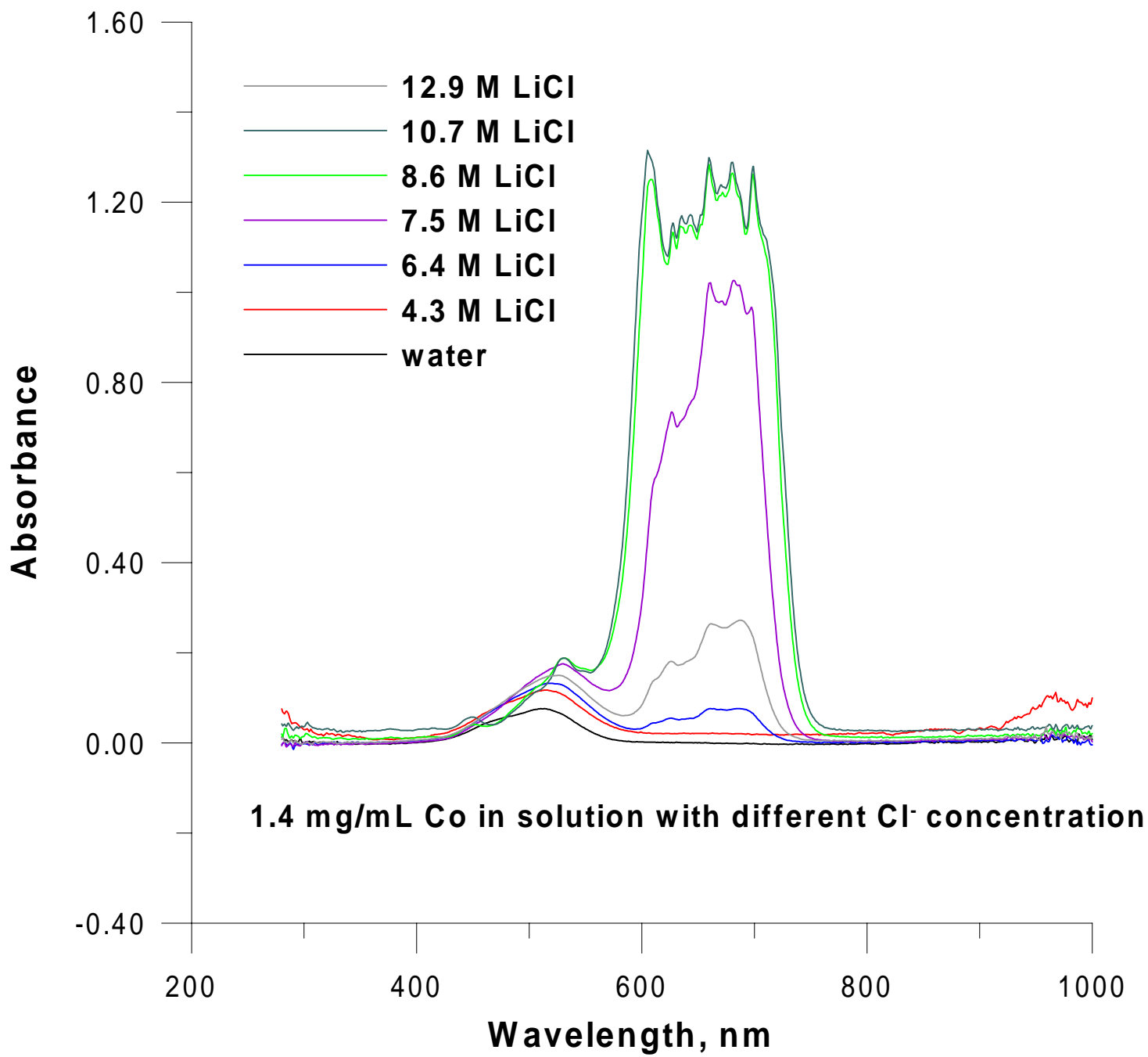


Figure 5a: Spectra of CoCl₂ in Various Concentrations of LiCl

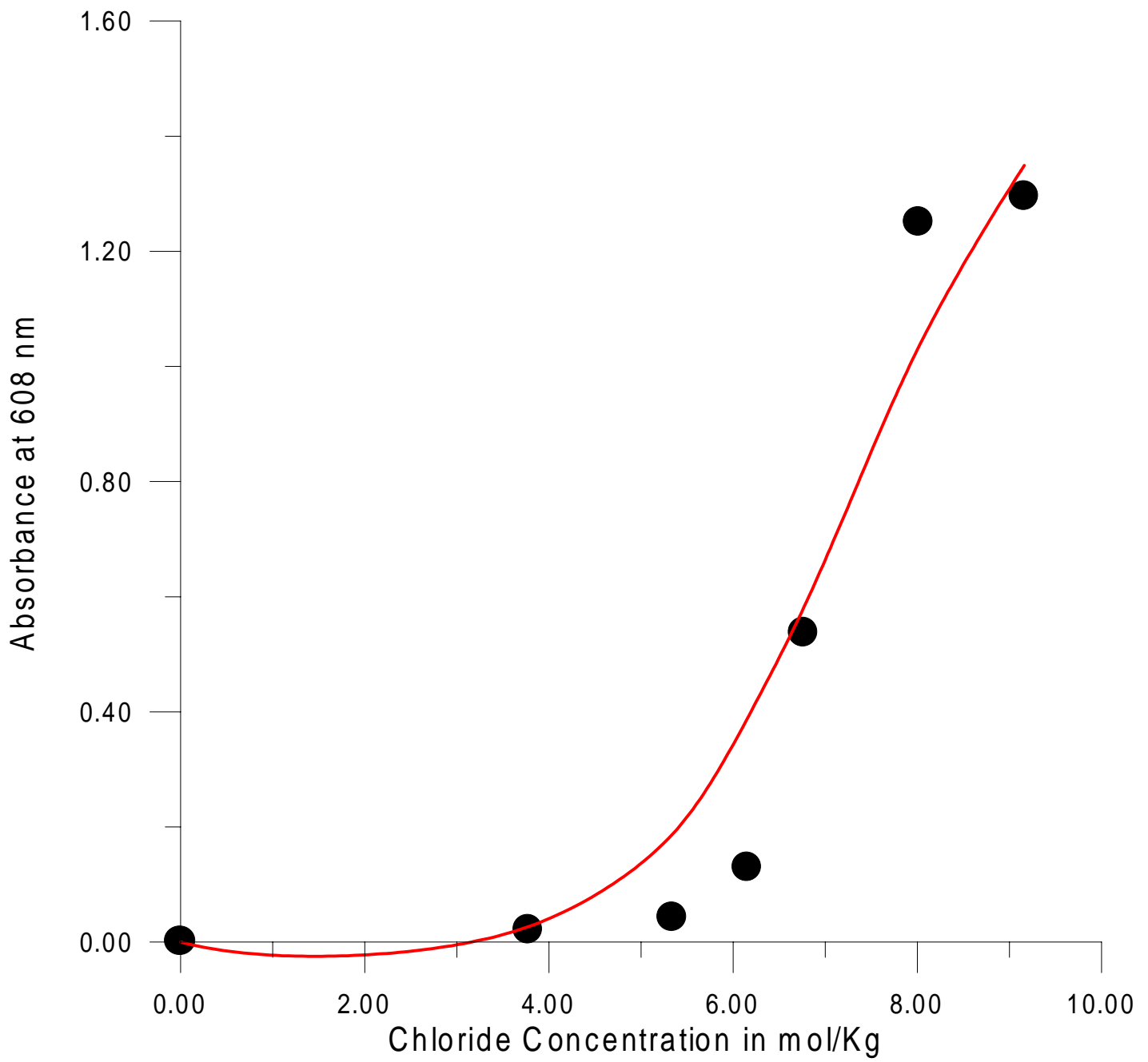


Figure 5b: Cobalt(II)-Chloride Complexation Model

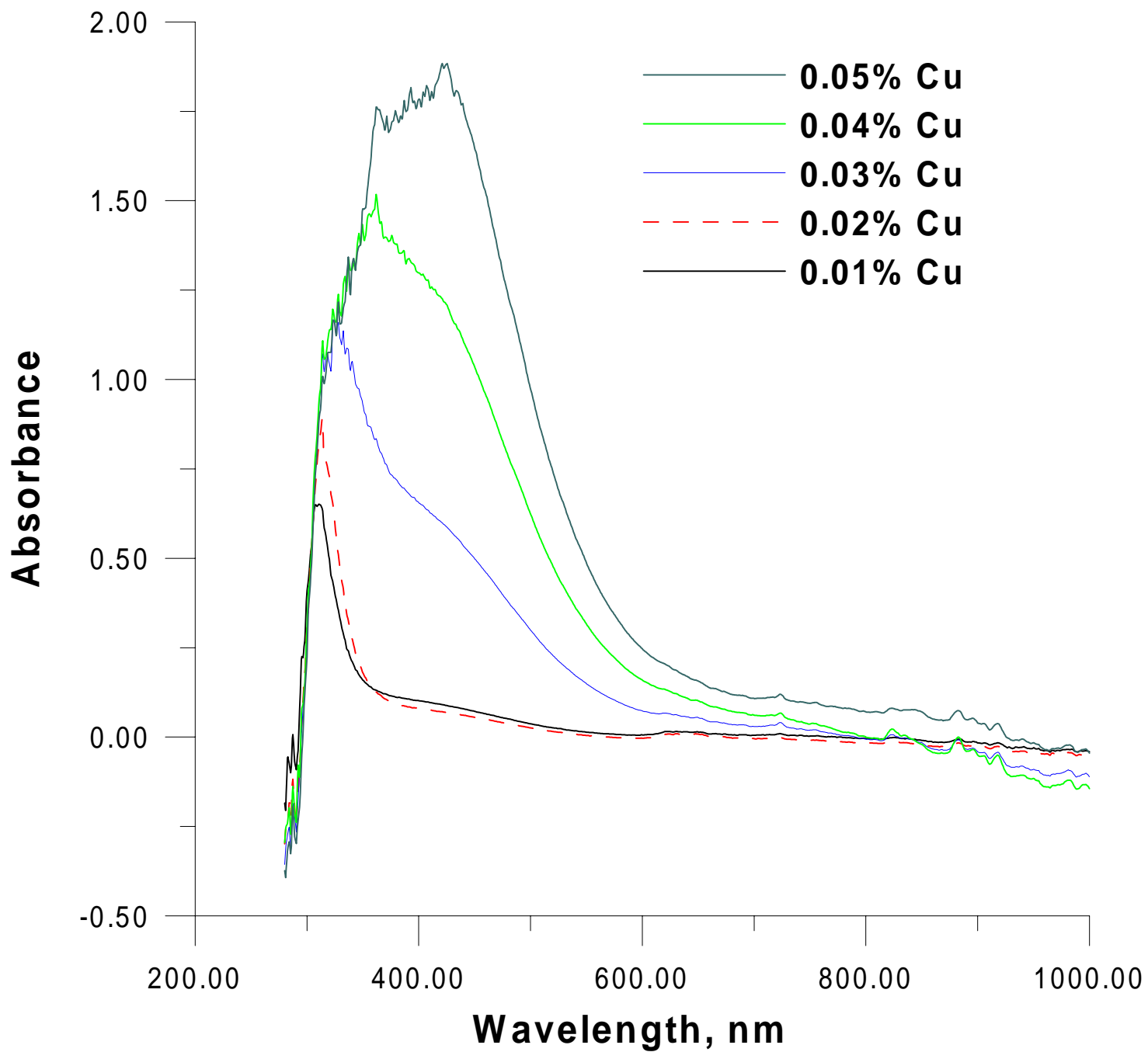


Figure 6a: Spectra of CuCl_2 in NaCl-KCl Melt Immediately after Melting at Various Concentrations of Cu(II)

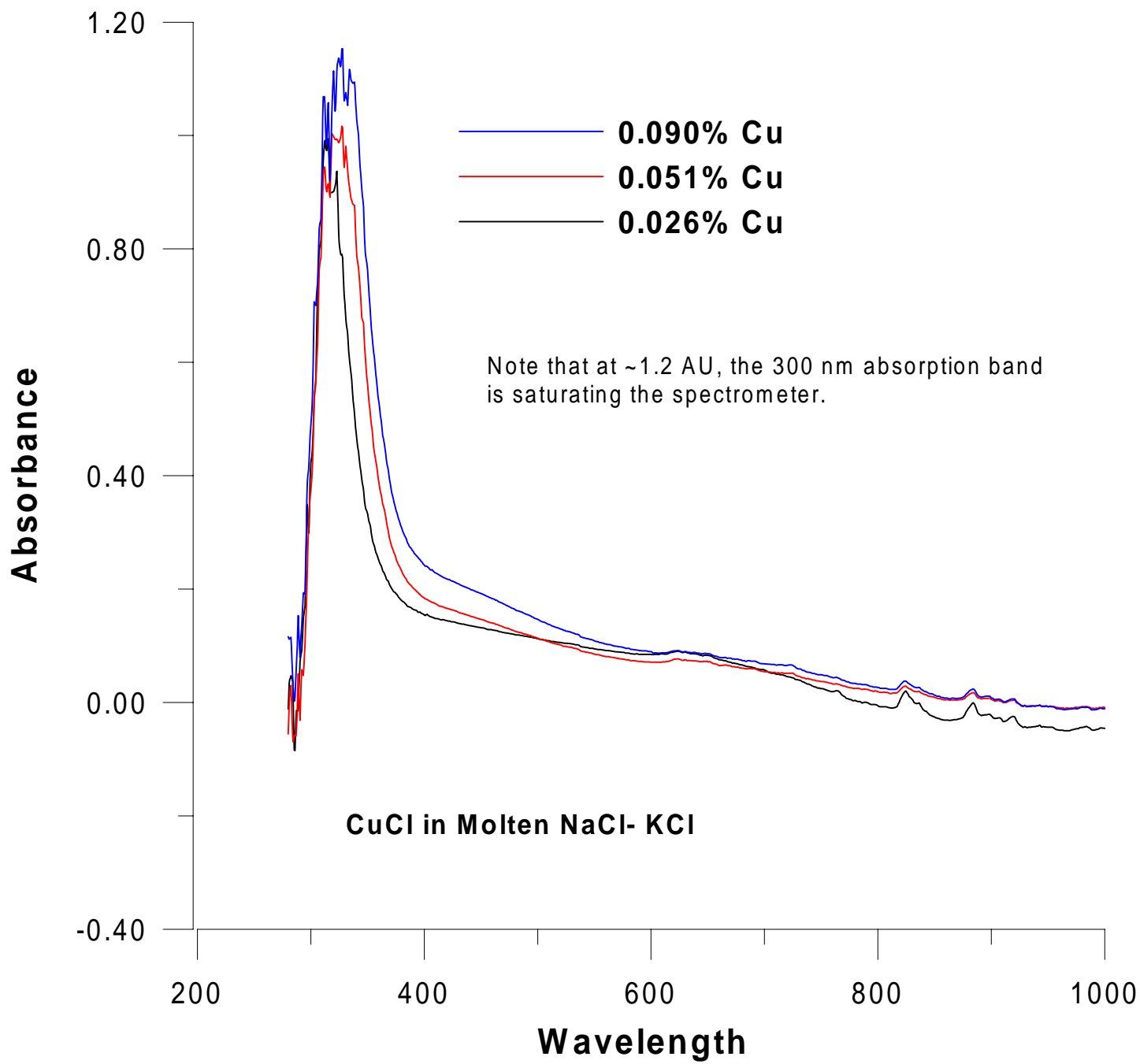


Figure 6b: Spectra of CuCl in Molten NaCl-KCl

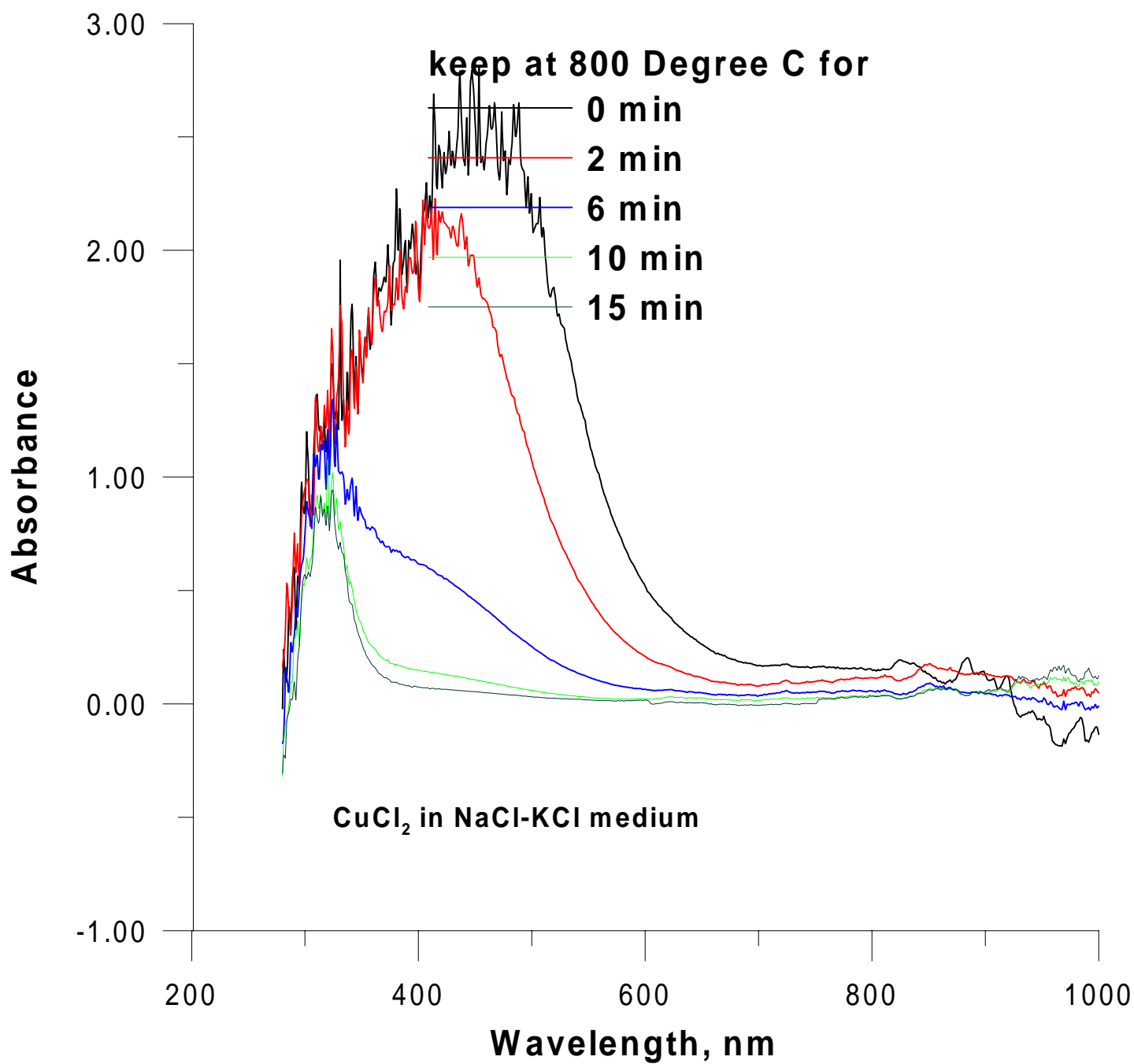


Figure 6c: Change in Spectral Characteristics of CuCl_2 after Holding for Various Periods at 800°C

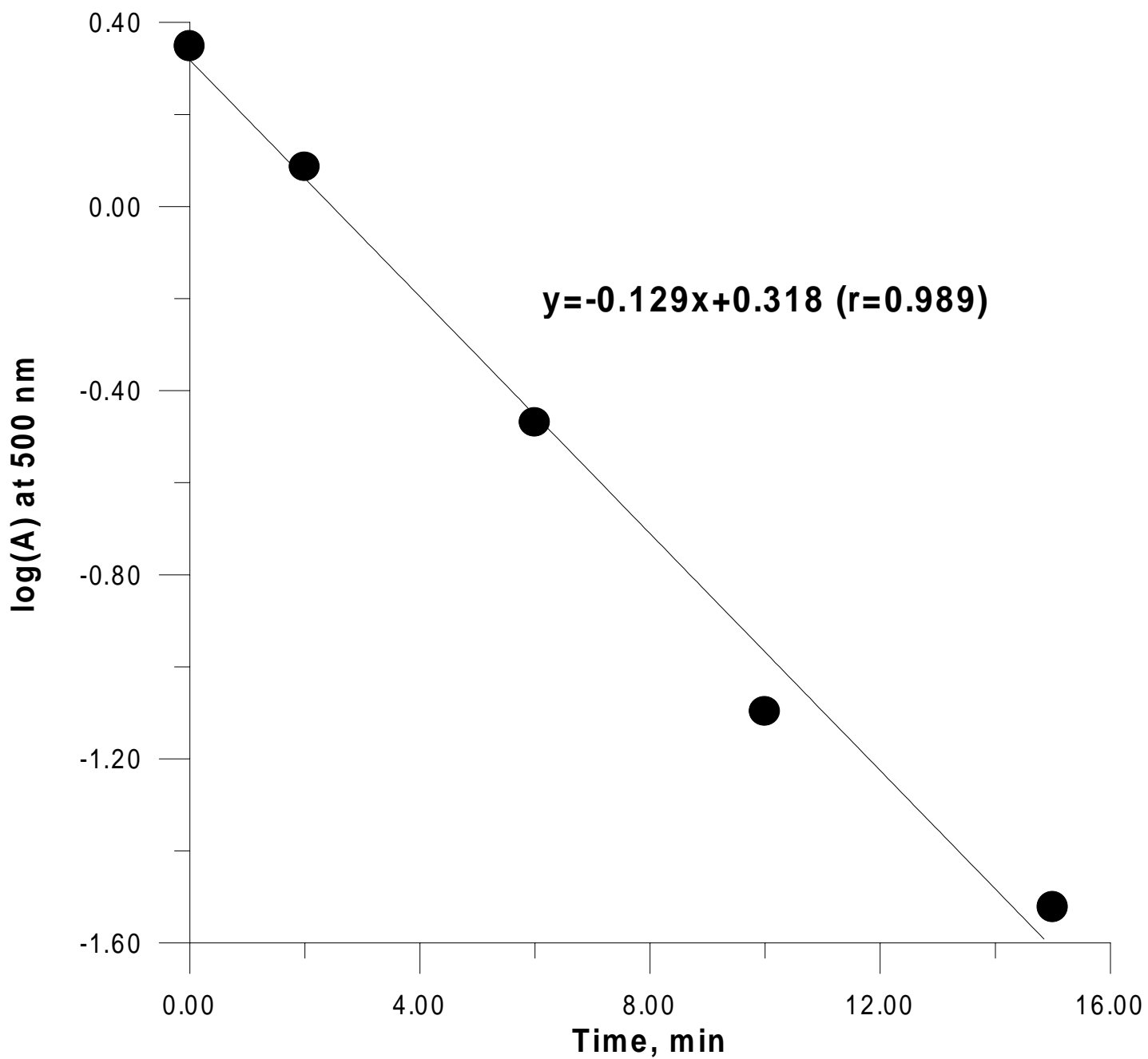


Figure 6d: First Order Decomposition Data for CuCl_2

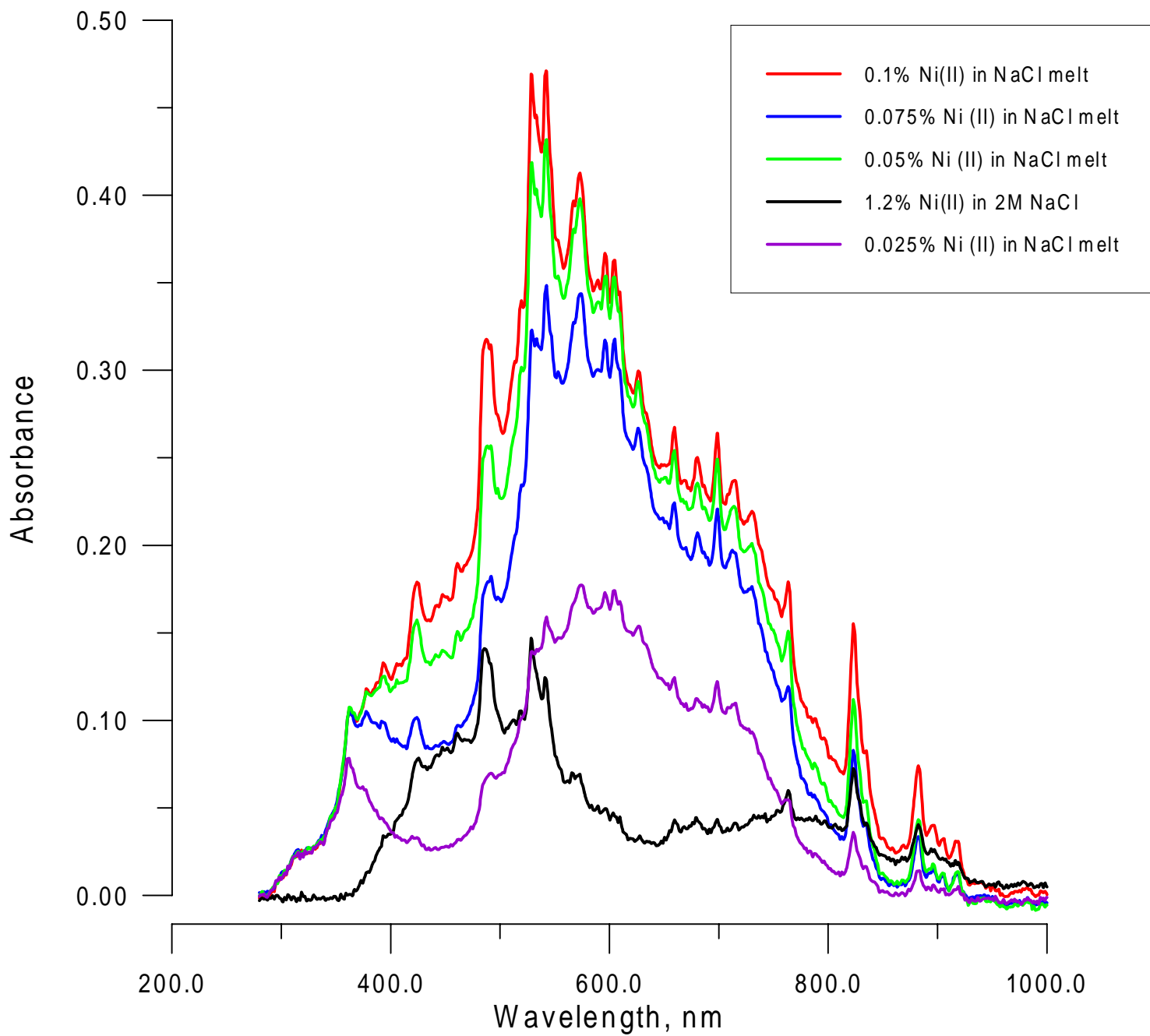


Figure 7: Spectra of NiCl₂ in NaCl Melt and in 2 M NaCl Solution